Available online at www.sciencedirect.com
ScienceDirect
Remote Sensing of Environment 105 (2006) 98–114
Remote Sensing of Environment
www.elsevier.com/locate/rse

The impact of gridding artifacts on the local spatial properties of MODIS data: Implications for validation, compositing, and band-to-band registration across resolutions

B. Tan [a,*], C.E. Woodcock [a], J. Hu [a], P. Zhang [a], M. Ozdogan [b], D. Huang [a], W. Yang [a], Y. Knyazikhin [a], R.B. Myneni [a]

[a] *Department of Geography and Environment, Boston University, 675 Commonwealth Avenue, Boston, MA 02215, USA*
[b] *NASA Goddard Space Flight Center, Greenbelt, MD, USA*

Received 4 May 2005; received in revised form 22 May 2006; accepted 18 June 2006

Abstract

Gridding artifacts between observations and predefined grid cells strongly influence the local spatial properties of MODIS images. The sensor observation in any grid cell is only partially derived from the location of the cell, with the average overlap between observations and their grid cells being less than 30%. This mismatch between grid cells and observations has strong implications for the use of reference data for the validation of MODIS products or the training of MODIS algorithms. When generating multidate composites, gridding artifacts introduce bias when spectral compositing criteria are used. Also, results indicate that the ability to generate consistent long-term remote sensing records is dependent on both consistent sensing scenarios (spectral bands, view angle distributions, geolocation error) as well as consistent compositing approaches. The band-to-band registration for the different spatial resolutions of gridded MODIS data can be poor if the different resolutions of data are gridded before aggregation. In all cases it is imprecise to characterize the subpixel properties of the coarser resolution bands using the finer resolution bands due to poor correspondence in the areas from which the observations are derived. All of the band-to-band registration problems are minimized when the MODIS data are aggregated to coarser resolutions. When validating algorithm accuracy, available data on the observation dimensions and the offsets between the grid cell and the observation should be included to ensure the quality of validation results. If this information is not available, MODIS data should be aggregated to coarser resolutions to improve the correspondence between the location of observations and grid cells.

Index Terms: Moderate resolution imaging spectroradiometer (MODIS); Gridding artifacts; Geolocation; View zenith angle; Triangular Point Spread Function (PSF); Band-to-band registration; Compositing; Validation

1. Introduction

The moderate resolution imaging spectroradiometer (MODIS) sensor onboard the Terra and Aqua platforms marked the beginning of a new era in remote sensing of the Earth, as in addition to the original data from the sensor there are a whole suite of derived products made freely available. Some products are more fundamental and provide radiometric properties (such as surface reflectance), while others involve more complex algorithms to provide estimates of surface properties or processes and may require inputs beyond the radiometric data from MODIS, such as climate data. All of the products are produced on a systematic basis globally and are made freely available (Justice et al., 2002). What is particularly revolutionary about this approach is the fact that the derived products are used much more frequently than the original observations. Since these products are used widely, it is important to determine their accuracy.

The accuracy of MODIS products is determined primarily through comparison with field measurements (Liang et al., 2002; Morisette et al., 2002; Privette et al., 2002; Tan et al., 2005; Wan et al., 2002; Wang et al., 2004). It should be noted that there are (at least) two types of validation activities for

* Corresponding author. Tel.: +1 617 353 8845; fax: +1 617 353 8399.
E-mail address: tanbin@crsa.bu.edu (B. Tan).

0034-4257/$ - see front matter © 2006 Elsevier Inc. All rights reserved.
doi:10.1016/j.rse.2006.06.008

satellite products. The first is to assess the satellite product accuracy independent of the observations from which they are derived. In this approach the products are viewed much like maps and can have both attribute error and locational error and there is not necessarily any effort to determine the source of the errors. The errors could be due to a wide variety of sources including imperfections in the observations, their registration, and imperfections in the algorithms used to generate the products. In this paper, we refer to this approach as "product validation." A second approach is to evaluate the algorithm accuracy. In this approach an attempt is made to quantify the contribution to product error arising due to imperfections in the algorithm. In this paper, we refer to this approach as "algorithm validation."

For both product and algorithm validations, a pixel-by-pixel comparison between MODIS data and reference data (which could be field measurements or fine resolution maps generated from field measurements and high-resolution satellite data) is common (Morisette et al., 2002). In previous validation studies, the misregistration of reference data has been considered. A patch level comparison rather than a pixel level comparison was performed to minimize the impact of the misregistration of reference field data/high-resolution satellite data. (Tan et al., 2005; Tian et al., 2002; Wang et al., 2004). However, the impact of misregistration between MODIS products and reference data has not been quantitatively evaluated. For "product validation", this source of misregistration is simply part of the product, and hence need not be considered separately from other sources of error. However, for "algorithm validation" it is important to ensure that the reference data are derived from the same location as the observations that form the basis of the MODIS products.

Griddling artifacts, first explained by Wolfe et al. (1998), are one source of MODIS misregistration error. They are introduced when sensor observations are assigned to the predefined system of grid cells. The gridding artifacts come from two effects: (a) the mismatch between the location on the ground from which MODIS observations are derived and the predefined grid cells for storing the observations, which is due to the use of a nearest neighbor resampling method and defined here as "pixel shift"; and (b) errors in assigning geolocation coordinates to observations, which are referred to as "geolocation error". The geolocation error has been quantified, and is modest (50 m at 1 sigma at nadir) (Wolfe et al., 2002). However, the combined effect of pixel shift and geolocation error has yet to be quantified and its implications explored. It should be noticed that pixel shift effects exist in all resampled satellite data regardless of the resampling method.

Although MODIS was designed to provide near-daily global coverage, the availability of MODIS data is reduced by the presence of clouds and atmospheric contamination. A commonly used approach to remove or reduce such problems is to composite data from multiple days into a single data set (Holben, 1986; Los et al., 1994). One critical assumption in the compositing process is that the repeated satellite observations cover the same area. However, this assumption is compromised by gridding artifacts that undermine the correspondence between observations and grid cells. The mismatch between observations and grid cells increases as view zenith angle increases because the size of the observations increases while the size of grid cells remains unchanged (Wolfe et al., 1998). Therefore, the "pixel shift" effect is primarily due to the size difference between observations and cells when view zenith angle is significant.

Few studies have investigated the bias in biophysical parameters resulting from misregistration in composited data. Moody and Strahler (1994) found that the maximum NDVI compositing method leads to a positive NDVI bias in composited AVHRR data. Roy (1997) compared the maximum NDVI and the maximum surface temperature compositing method on AVHRR data and found that the compositing procedure influences significantly the distribution of the NDVI and surface temperature values. NDVI values are higher using the maximum NDVI method than from the maximum surface temperature method. He also indicated that inappropriate selection of a compositing method may have a significant impact on the subsequent application of the derived biophysical parameters.

In this paper, the effect of different compositing methods is investigated on MODIS data through simulation. The NDVI values of simulated 8-day composites resulting from different compositing methods are compared with reference NDVI values.

MODIS makes observations of the Earth in three at-nadir spatial resolutions: 250-m (Bands 1–2); 500-m (Bands 3–7), and 1-km (Bands 8–36). Following the terminology used by Roy (2000), an *observation* refers to the measurement made by a detector and the observed surface size is referred to as the *observation dimensions*. The size of the grid cells used to store the observations matches the size of observations at nadir. This paper investigates the relationship between gridding artifacts and MODIS data quality and has three objectives: (1) to quantify the degree of correspondence between the predefined MODIS grid cells and the MODIS observations used to fill them; (2) to evaluate bias in MODIS multidate composites due to gridding artifacts using various compositing strategies; and (3) to assess the band-to-band registration between the different resolutions of MODIS data.

2. Data

To estimate the effects of gridding artifacts, a simulation approach is used because of the following advantages: (a) the impact of view zenith angles on MODIS data quality and gridding artifacts can be quantitatively evaluated; (b) the baseline data is a precise reference for evaluating MODIS data quality. In this study, Landsat ETM+ data are used as baseline data to generate simulated MODIS data.

2.1. Landsat ETM+ data

To investigate the impact of gridding artifacts for different ground situations, six Landsat ETM+ images were used to simulate MODIS data — summer and winter (or early spring) scenes for Harvard Forest (HF), the Konza Prairie LTER (KP), and Lake Tahoe (LT) (Table 1). The land cover types of these three sites are mixtures of broadleaf and needle leaf forests, grass and cereal

Table 1
The information of ETM+ data used in this study

Site	Path	Row	Date	Land cover types
Harvard Forest	13	30	2001-09-05 2002-02-28	Mixture of broadleaf forests and needle leaf forests
Konza Prairie LTER	28	33	2000-04-04 2000-07-09	Grasses and cereal crops
Lake Tahoe	43	33	2000-08-19 2001-02-27	Needle forests

crops, and needle leaf forests, respectively. Each ETM+ subset has a spatial resolution of 30 m and covers a 147 by 147 km region, stored in the Universal Transverse Mercator (UTM) projection. The ETM+ data have six bands — Band 1 (blue, 450–515 nm), Band 2 (green, 525–605 nm), Band 3 (red, 630–690 nm), Band 4 (near-infrared (NIR), 780–900 nm), Band 5 (1550–1750 nm) and Band 7 (2090–2350 nm). The images were atmospherically corrected using Dark Object Subtraction (Song et al., 2001).

2.2. MODIS data

Collection 4 Terra MODIS products are used to verify the simulation results. The Collection 4 MODIS products are projected on the Sinusoidal 10-degree grid, where the globe is divided for production and distribution purposes into 36 tiles along an east–west axis, and 18 tiles along the north–south axis, each approximately 1200 by 1200 km. The surface reflectance products and observation pointer products are used in this study.

The Collection 4 MODIS observation pointer products are produced daily at 250 m, 500 m, and 1 km spatial resolutions. The 500 m resolution product (MODPTHM) from January 1st to February 19th of year 2004 in tile h18v04 near Alpilles, France and tile h12v04 near Harvard Forest, USA were used in this study. The observation pointer product records the geolocation relationship between ungridded observations and the grid cells, including the subpixel scan line offset, subpixel sample offset, and the intersection area of a grid cell and its observation (Wolfe et al., 1998). Detailed information on this product is available at MODIS land quality assessment website (http://landweb.nascom.nasa.gov/).

3. Methodology

ETM+ data were used as the baseline data to simulate MODIS data in this study. The key issue in the simulation process is to apply MODIS sensing characteristics to ETM+ data. Therefore, the MODIS characteristics to be simulated are introduced first, and then the simulation progress is described in detail. Lastly, the method used to quantitatively evaluate band-to-band registration is shown.

3.1. Wide field of view

The across-track scan angle of MODIS ranges from 0 to 55°. One MODIS scan line is composed of 1354 observations at 1 km, 2708 at 500 m, and 5416 at 250 m (Wolfe et al., 2002). The curvature of the earth elongates the scan line to approximately 2340 km (Wolfe et al., 1998) and makes the view zenith angle larger than the scan angle. At the end of a scan line, the view zenith angle can be as large as 65°. The observation dimensions of MODIS data increase as view zenith angle increases (Fig. 1). The increasing observation dimensions lead to two effects in MODIS data. First, consecutive scan lines overlap each other when view zenith angle is larger than 0°. This overlap increases as the view zenith angle increases to a maximum of almost 50% at the end of a scan line. This is called the "bowtie" effect (see Fig. 2 in Wolfe et al., 1998). Second, individual observations cover several adjacent grid cells at high view zenith angles because the grid cell size of MODIS images is fixed at the same dimensions as the observation dimensions at nadir (Justice et al., 2002). The quality of MODIS data is degraded at high view zenith angles.

3.2. Triangular point spread function

In the simulation process the PSF of MODIS cannot be neglected. The sensor PSF includes several components: the optical PSF, the image motion PSF, the electronic PSF, and the detector PSF (Schowengerdt, 1997). The image motion PSF, which is caused by the motion of the scan mirror during the measurement time integration, determines the observation dimensions and is the most important component of the MODIS sensor PSF in the along-track direction. The PSFs due to optics, electronics and the detectors will expand the actual observation area in both along-scan and along-track directions, and smooth the triangular image motion PSF in the along-track direction (see Fig. 3 in Barnes et al., 1998). The blurring effect of these factors and the atmosphere are different for 250 m, 500 m, and 1 km MODIS data and vary as a function of scan angle and earth curvature. They are not included in this study because their effects are small compared with the image motion PSF and are not the primary concern here. It is worth noting that since all the factors not included would tend to accentuate the magnitude of

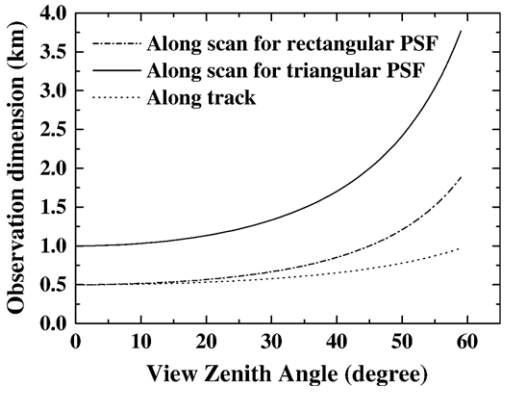

Fig. 1. The observation dimensions as a function of view zenith angles (VZA). The nominal observation size at nadir is 500 by 500 m. The size changes in the along-track direction, where the sensor point spread functions (PSF) is rectangular, are shown as the dot line. In along-scan direction, the size changes are shown as a dashed line when the sensor PSF is assumed to be rectangular, and a solid line for the more realistic triangular PSF (derived from Fig. 2 in Wolfe et al., 1998).

gridding artifacts such that the results presented here are the best-case scenario.

What the sensor measures in one observation can be written as the following (Schowengerdt, 1997):

$$F_\lambda = \int\int_D w(x,y) f_\lambda(x,y) \mathrm{d}\sigma \quad (1)$$

where F_λ is the electronic signal collected from one observation at spectral band λ; D represents the observed ground area; σ is the sample area($\sigma \in D$); w is the sensor PSF function acting as the weighting function for a spatial convolution; f_λ represents the spatial distribution of the radiance from the ground. Both w and f_λ depend on the location (x,y) in the observation. Here the x direction is the along-scan (or across-track) direction and the y direction is the along-track direction. Eq. (1) can be written as the following when the observation area is a rectangle with along-scan dimension ψ, along-track dimension Φ, and the observation center at (x_0, y_0):

$$F_\lambda = \int_{y_0-\frac{\Phi}{2}}^{y_0+\frac{\Phi}{2}} \int_{x_0-\frac{\Psi}{2}}^{x_0+\frac{\Psi}{2}} w(x-x_0, y-y_0) f_\lambda(x,y) \mathrm{d}x\mathrm{d}y \quad (2)$$

At nadir, the MODIS detectors receive a signal at any particular instant from a square area of the Earth's surface that is 250 m, 500 m, or 1 km on a side. The MODIS sensor PSF would be approximately rectangular (Fig. 2a), much like the Landsat ETM+, if the MODIS detectors collected the signal from one single pixel, then moved to the next pixel. In such a case, w is:

$$w(x,y) = \begin{cases} 1 & (x,y) \in D \\ 0 & \text{otherwise} \end{cases} \quad (3)$$

where D is the rectangle observation area centered at (x_0, y_0) with along-scan dimension (ψ) and along-track dimension (Φ). However, this is not the case for MODIS. In the along-scan direction, the linear dimension of the area sensed is twice as long as the nominal observation size, and the MODIS sensor PSF is triangular as shown in Fig. 2b. In the along-track direction, the PSF is still approximately rectangular (Barnes et al., 1998; Nishihama et al., 1997). In such a case, w is:

$$w(x,y) = \begin{cases} \Psi - |x-x_0| & (x,y) \in D \\ 0 & \text{otherwise} \end{cases} \quad (4)$$

The triangular PSF results in overlap between adjacent observations such that 25% of the signal is from adjacent nominal observation areas, while only 75% comes from the corresponding nominal observation area (Fig. 2b). The observation size also increases as the view zenith angle increases (Fig. 1).

3.3. The gridding process

The primary source of gridding artifacts is "pixel shift", which is introduced in the MODIS gridding process. Gridding is defined as assigning sensor observations to grid cells (Wolfe et al., 1998). The coordinates of the grid cells are predefined by specifying the cell dimensions and the origin and orientation of the grid cells globally. For MODIS, the grid is defined using a Sinusoidal projection. The observations from any particular overpass and the grid cells are mismatched as they have different dimensions and are misaligned. We refer to this mismatch as "pixel shift". To quantitatively describe pixel shift, Wolfe et al. (1998) defined the term obscov, which was initially defined as the ratio of the intersection area (S_0), between the nominal observation and the grid cell, over the nominal area of the observation (S_2):

$$\mathrm{Obscov}_{\mathrm{old}} = S_0 / S_2 \quad (5)$$

Using this definition, obscov does not accurately represent the relationship between a grid cell and its observation due to the effects of the triangular PSF. Therefore, in the most recent version (Collection 4) of MODIS data, obscov is redefined as the integrated response over the observation/grid cell intersection area divided by the integrated response over the area of the observation footprint (Yang & Wolfe, 2001):

$$\mathrm{obscov} = \frac{\int\int_{D'} w(x-x_0, y-y_0) \mathrm{d}\sigma}{\int\int_D w(x-x_0, y-y_0) \mathrm{d}\sigma} \quad (6)$$

where D' is the observation area overlapped by the grid cell. Obscov is an extremely helpful descriptor of the gridding and aggregation processes and can be thought of as the proportion of an observation derived from the area of the grid cell to which it is assigned.

Two gridding algorithms, simple and complex, are applied for MODIS products. The simple method stores all observations from a single day that overlap a cell without changing the original observation values. The observations are ranked according to obscov. The highest ranking observation of each cell becomes the first layer of the MODIS surface reflectance data, and the remaining observations for each cell comprise of the

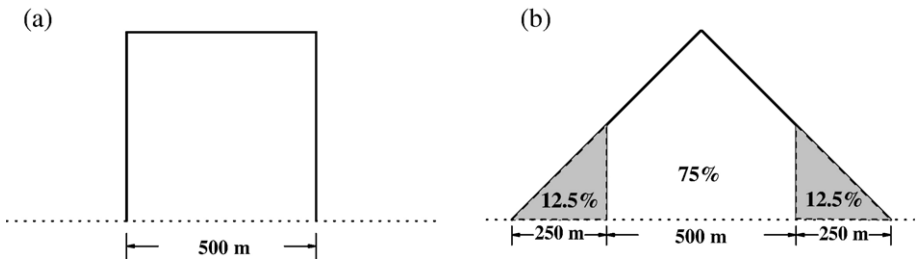

Fig. 2. Sensor point spread functions (PSF) (examples at 500 m resolution): (a) an idealized rectangular PSF in which the nominal observations agree with the actual observations; and (b) the triangular PSF which better models that of MODIS, in which the nominal observation area contributes 75% of the actual observation. (Fig. B is derived from Fig. 2–6 in Nishihama et al., 1997).

subsequent layers. This method is essentially a nearest neighbor resampling method (Wolfe et al., 1998). MODIS surface reflectance products (the MOD09 series of products whose native resolution is 250 m or 500 m) use this algorithm. Collection 5 MODIS land surface temperature products (MOD11 series products whose native resolution is 1 km) will use this algorithm too, but only the first layer (or the observation with the highest obscov) value is stored.

The complex method, instead of storing the original observation values as it comes from the sensor, calculates a value for a grid cell by weighting all observations overlapping this cell according to their obscov values. Therefore, only a single layer results from the complex methods. Collection 4 MODIS land surface temperature products use the complex method in gridding.

3.4. The aggregation process

In addition to providing MODIS bands at their original resolutions, the 250 m bands are also provided at 500 m. Similarly, all bands are provided at 1 km. An aggregation process is used to create these products. Similar to the gridding process, the aggregation algorithms can be divided into simple and complex methods.

The simple method is to average all fine resolution grid cells in the first layer that fall into a coarse resolution cell. All fine resolution cells have the same weighting. This is a commonly used method when users of the satellite data generate coarse resolution data sets themselves. Therefore, we include this method in this research though there are no longer any MODIS products that use this aggregation method.

The complex method utilizes all observations falling into the fine resolution cells that intersect a coarse resolution cell. The observations are averaged using a weighting scheme based on obscov values. The 1 km surface reflectance product, named MODIS Level 3 1 km Land Surface Reflectance Aggregation product (MODAGAGG), uses the complex aggregation method. Bands 1–2 of MODAGAGG are aggregated from native 250 m data, while bands 3–7 are from native 500 m data. In this process, 4×4 cells of 250 m observations (or 2×2 cells of 500 m observations) from the MODIS L2G surface reflectance product are aggregated to produce a single reflectance value (for each band) for the 1 km cell. Observations from different orbits are aggregated separately to retain consistent sun and view geometry characteristics.

3.5. Simulation of the MODIS gridding and aggregation processes

Each of the six ETM+ subsets, 147 by 147 km, was duplicated 9 times and mosaiced side-by-side to produce half a MODIS swath (see Fig. 6). In the along-track direction, the mosaiced ETM+ scenes cross 147 km. We did not simulate a full swath because the MODIS swath is symmetrical to its orbit (Fig. 2 in Wolfe et al., 1998). Therefore, with half a swath the simulation can represent all the required characteristics of MODIS data.

To simplify the simulation process, four assumptions were made: (1) the spatial variability due to the sensor PSF of 30 m ETM+ pixels may be neglected with respect to the spatial variability of coarse resolution MODIS data; (2) the PSF of ETM+ data due to the atmosphere is neglected; (3) the orientations of the observations and grid cells were in perfect alignment at nadir; (4) the geolocation error for the observations in one simulated orbit is constant. Because of assumptions (1) and (2), ETM+ data may be regarded as ground truth i.e. punctual surface radiometric data. Assumptions (3) and (4) are for simplifying the simulation process.

Fig. 3 illustrates the process to generate simulated daily MODIS data. We simulated a series of steps beginning with the location of the sensor and its measurements through the production of gridded MODIS data. Therefore, the simulation generates observations first, and then assigns the observations to a grid of cells according to the following four steps.

The first step is to determine the orbit positions. Initially, one orbit position is randomly selected in the joint ETM subsets. The positions of adjacent orbits are determined according to the distance between two real adjacent orbits at 45° latitude (approximate 1980 km). The orbit positions for the following simulated days are determined by the real temporal Terra orbit pattern (Appendix 1). After determining the orbit position, the initial satellite position in the along-track direction is randomly selected through a uniform random function.

The second step is to calculate the center and the dimensions of each simulated "MODIS" observation. The scan angle of each "MODIS" observation is derived from the height of the satellite (705 km) and the known orbit position (determined in the previous step). The observation dimensions at nadir are known (250 m, 500 m, and 1 km). Therefore, the center and the dimensions of each simulated MODIS observation can be derived from observation dimensions at nadir and the scan angle (Appendix 2). This step generates an "observation layer" that is intended to simulate what MODIS measures (Fig. 3).

The third step is to generate simulated "ungridded MODIS observations". The "observation layer" is overlaid on the ground truth (ETM+ data as mentioned before) (Fig. 3). For each simulated observation, the weighted mean of all ETM+ pixels falling into this observation is considered as the observed value of this simulated MODIS observation. This progress is described by Eqs. (2) and (4) in Section 3.2. The last step is to place the ungridded MODIS observations into a predefined grid of cells, a process known as "gridding" in processing real MODIS data. It should be noted that there are two types of overlap between scan lines: first, consecutive scan lines from the same orbit overlap towards high view zenith angles, second is at the end of scan lines, the observations from different orbits overlap. At 45° latitude, the scan lines from adjacent orbits begin to overlap when the scan angle is greater than 47° from nadir (view zenith angle greater than 55°). The length of the overlapped area in along-scan direction is approximate 360 km. Therefore, the grid cells in the overlap area may get their values from different scan lines', even different orbits', observations. There may be offsets between the observations and cells — "pixel shift" (refer to Section 3.3). The simple and complex

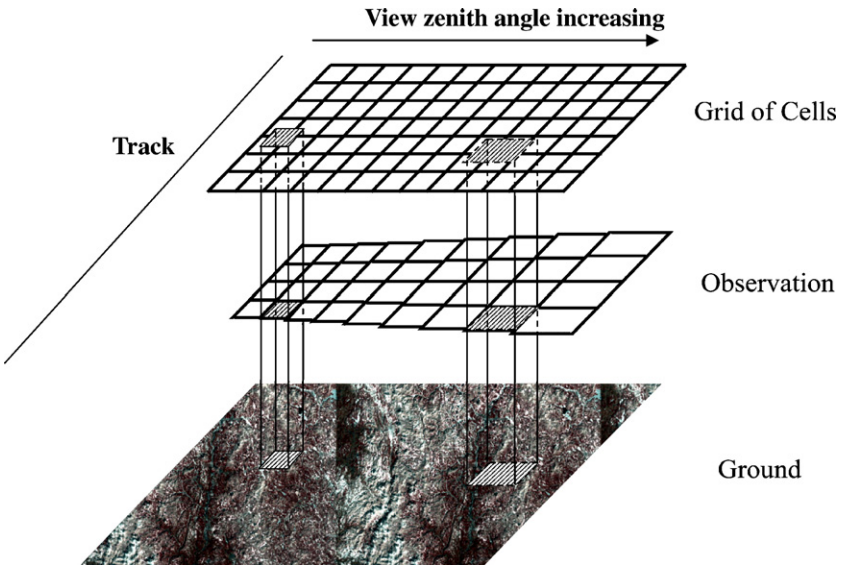

Fig. 3. The simulation process applied in this study. The ETM+ data (30 m spatial resolution) is considered as ground truth. The simulated MODIS observations have to be matched to a predetermined grid of cells. A cell gets its value from the observation which covers the cell the most (nearest neighbor resampling method). For large view zenith angles, one observation will be allocated to multiple cells. There may be offsets between the observations and cells (we call this "pixel shift") depending on the position of the satellite and the dimensions of the observations. In addition to the "pixel shift" there is also a geolocation error (50 m at 1 sigma, refer to Wolfe et al., 2002).

gridding methods (Section 3.3) are applied to generate two sets of gridded data sets. At nadir, the nominal observation size is equal to the dimensions of a grid cell. The magnitude of pixel shift in along-track/along-scan direction is $[-L/2, L/2]$ (Fig. 3), where L is the nominal observation dimensions at nadir. Toward the end of the scan line, the magnitude of pixel shift increases as the observation dimensions increase (Figs. 1 and 3). On top of the "pixel shift", another factor "geolocation error", introduced when the sensed observations are geolocated, influences the gridding process. Geolocation error in MODIS data has been previously quantified at 50 m at 1 sigma at nadir (Wolfe et al., 2002). In the simulation, the geolocation error was randomly selected through a normally distributed random function with 50 m at 1 sigma. This geolocation error was applied to the location of observations. The relative geolocation errors between adjacent observations and between consecutive scan lines were assumed to be negligible. However, the geolocation errors for the observations/scan lines from different orbits were different. This is because the geolocation error changes with the viewing geometry and varies with time in the sensor position and attitude (Roy et al., 1997).

To assess the attributes of multidate composites, eight days of simulated MODIS data were generated from the same ETM+ data with the previously defined temporal orbit pattern and gridding artifacts. Three composting methods, maximum Normalized Difference Vegetation Index (NDVI), minimum blue reflectance, and minimum view zenith angle (VZA) were used to generate composites from the simulated daily data. In the MODIS compositing process, the cloud mask is used to eliminate poor quality pixels. However, the cloud problem is not considered in this study because all of the ETM+ data used are cloud free or include negligible amounts of clouds.

The impact of gridding artifacts on MODIS data is similar for 250 m, 500 m and 1 km data. However, the bow-tie effect imposes slightly different gridding artifacts in the data with different native resolutions in the along-track directions between consecutive scans. In the along-track direction, the overlapped dimension between consecutive scan lines begins to be larger than the observation dimensions when the view zenith angle (scan angle) is approximate 19° (17°) for 250 m data, approximate 27° (24°) for 500 m data, and approximate 39° (34°) for 1 km data. Therefore, towards the end of the scan lines, the grid cells receiving their observations from consecutive scan lines happen first in 250 m data, then in 500 m data, and last in 1 km data. In this research, the analyses of daily and 8-day-composite data quality only use the first layer of simulated 500 m resolution data as examples. The first layer is used because it has the best quality and some grid cells in the subsequent layers have no valid values. The observations with the maximum obscov value were stored in the first layer and the observations with progressively smaller obscov values were stored in the subsequent layers (second layer, third layer....) (Wolfe et al., 1998; Section 3.3). The number of observations per grid cell varies from nadir to the end of scan lines, and from one scan line to another depending on the latitude where the data are collected.

To quantitatively assess simulated MODIS data quality, a set of reference data is generated. The reference data is produced in seven bands without view geometry and triangular PSF effects. The spatial resolution of the reference data is the same as the simulated MODIS data, but without gridding artifacts. In essence, the reference data represents the best quality satellite data possible at the spatial resolution of the simulated MODIS data.

3.6. Quantitative evaluation of band-to-band registration

To investigate the quality of band-to-band registration, the 250 m simulated MODIS data are aggregated to 500 m and

1 km, and 500 m simulated MODIS data are aggregated to 1 km. Both the simple and complex methods are separately applied in aggregation.

In the along-track direction, the sensor PSF is approximately rectangular. A 1 km observation covers exactly two 500 m observations and four 250 m observations. The normal aggregation method of averaging four 250 m observations (or two 500 m observations) to a 1 km observation is appropriate. However, the situation in the along-scan direction is not as straightforward because the sensor PSF is triangular in the along-scan direction (refer to Section 3.2). Fig. 4a shows the registration of 250 m, 500 m and 1 km MODIS observations in the along-scan direction. A single 1 km observation covers the same area as three 500 m observations and seven 250 m observations. When aggregating 500 m resolution data to 1 km, two 500 m observations in along-scan direction are not enough

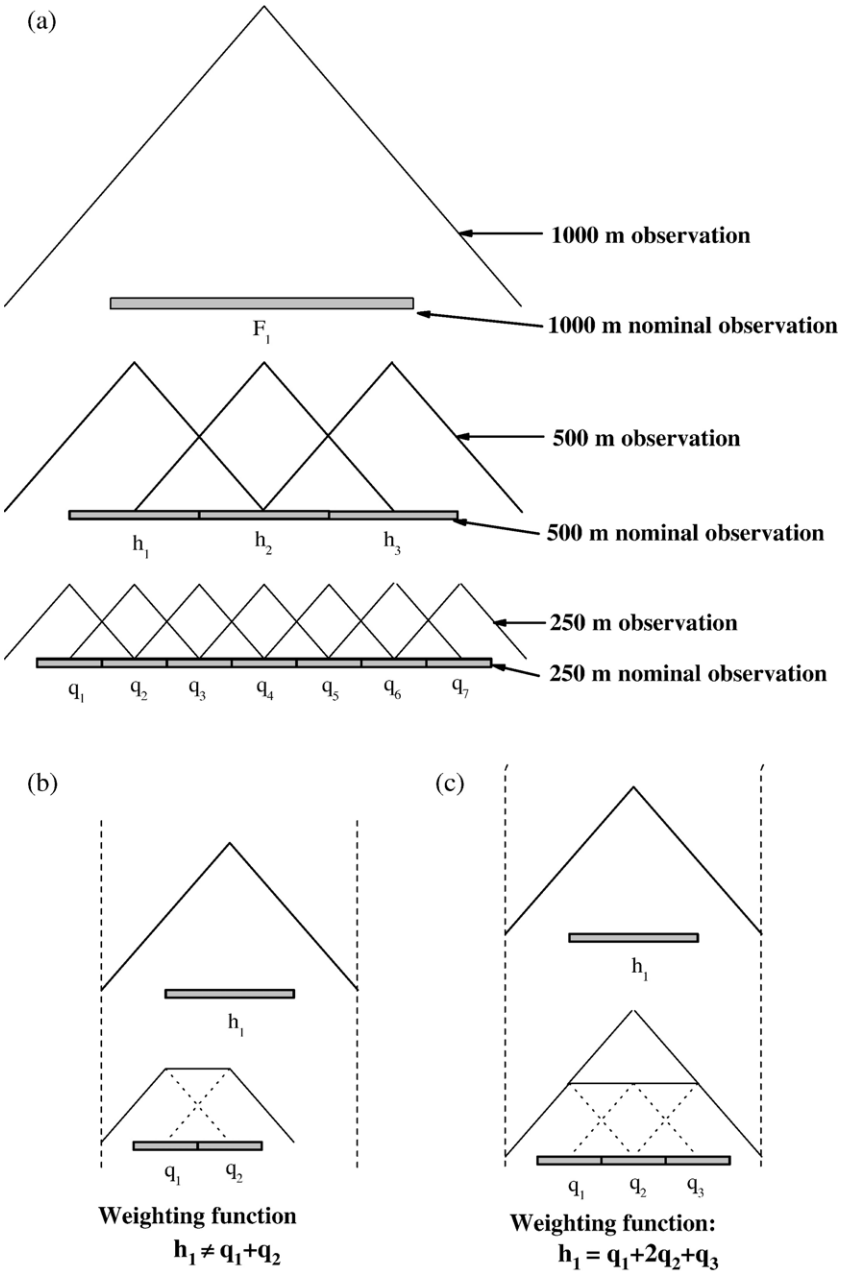

Fig. 4. (a) The registration of 250 m, 500 m, and 1 km MODIS observations. The figures show the PSFs of the various resolutions of MODIS data. The *x*-axis is simply distance, and the *y*-axis is the weighting of the PSF. When viewed from a linear perspective, a 1 km observation covers the same area as three 500 m observations and of seven 250 m observations. (b) The combination of two 500 m observations cannot be registered with one 1 km observation because they cover different ground areas. The correct method is shown in panel (c), which utilizes three adjacent 500 m observations with a set of weighting coefficients. Similarly, four 250 m observations cannot be aggregated to the corresponding 1 km observation. The proper way is to use seven 250 m observations with a set of weighting coefficients. It should be noticed that a 1 km pixel encompasses 2 × 3 500 m (or 4 × 7 250 m) pixels. In along-track direction, the sensor PSF is a rectangular and various resolutions of data are registered in a normal way (e.g., 1 1 km pixel covers exactly 2 500 m pixels) (This figure is derived from Fig. 2–7 and Fig. 2–9 in Nishihama et al., 1997).

because they cover a smaller area than a 1 km observation (Fig. 4b). The correct aggregation method should utilize three 500 m observations (h_1, h_2, and h_3) in the along-scan direction with a weighting function $h_1+2h_2+h_3$ (Fig. 4c), which results in the same weighting of the surface as a native 1 km resolution observation. Similarly, the correct aggregation method for 250 m observations should utilize seven observations ($q_1 \ldots q_7$) with a weighting function $q_1+2q_2+3q_3+4q_4+3q_5+2q_6+q_7$.

However, this aggregation scheme is not applicable to gridded MODIS data because the gridding process undermines the correspondence between coarse and fine resolution observations. In a gridded MODIS image, a 1 km cell covers 2×2 500 m cells and 4×4 250 m cells, which conflicts with the geometry of the observations, as described above. Therefore, there are two ways to generate MODIS products from data with different native resolutions: (1) aggregate the fine resolution observations to the coarser resolution and then grid the aggregated and native observations simultaneously; or (2) grid the different resolutions of data first, and then aggregate. In this scenario for example, 4×4 250 m cells or 2×2 500 m cells would be aggregated to produce a 1 km product. The MODIS products aggregated prior to gridding (the first approach), such as MOD09GHK, the 500 m surface reflectance product from 250 m and 500 m data retains perfect band-to-band registration. However, the products using the second approach, such as the MODIS Level 3 1 km Land Surface Reflectance Aggregation product (MODAGAGG), suffer misregistration due to gridding artifacts.

A variable, named the matching index (ξ), is introduced here to quantitatively evaluate the misregistration between two aggregated (or native) observations. It is defined as:

$$\xi = \left(V_{\sum\sum \alpha_j h_j}^{\sum \beta_i F_i} / V_{\sum \beta_i F_i} + V_{\sum\sum \alpha_j h_j}^{\sum \beta_i F_i} / V_{\sum \alpha_j h_j} \right) / 2 \qquad (7)$$

where $V_{\sum \beta_i F_i}$ is the integrated PSF of the weighted aggregation of observation F_i. $V_{\sum \alpha_j h_j}$ is the integrated PSF of the weighted aggregation of observation h_j. The integrated PSF can be thought as the volume of the polygon above the observed surface with the heights of the vertices given by the product of the weighting coefficient and the sensor PSF value (derived from Yang & Wolfe, 2001). $V_{\sum\sum \alpha_j h_j}^{\sum \beta_i F_i}$ is the overlapped integrated PSF of two aggregations. The parameters α_i and β_j are the weighting coefficients applied in aggregation for the observation F_i and h_j respectively. For the simple aggregation method, the weighting coefficients are equal to 1. In the complex method, the weighting coefficient for observation F_m, α_m, is calculated as $\text{obscov}_{F_m} / \sum \text{obscov}_{F_i}$. The weighting coefficient β_n is calculated in a similar way. In essence, the matching index is the mean percentage of overlap of two aggregated (or native) observations divided by these two observations. The match index (ξ) equals 1 when two aggregations coincide exactly, and equals to 0 when there is no overlap between the two aggregations. Fig. 5 presents a simple case (a 1 km observation vs. two 500 m observations) for calculating ξ.

4. Results and discussion

4.1. The impact of gridding artifacts on observation-to-grid cell registration

The first layer of simulated MODIS data (from the simple gridding method, see Section 3.3), using the ETM+ data for the Konza Prairie LTER on April 04, 2000, is shown in Fig. 6. The spatial variability of MODIS data decreases as view zenith angle increases because the observation dimensions are significant greater than the cell size at the end of the scan line, and one observation value is allocated to as many as eight adjacent cells (Fig. 7). The observation dimensions at the end of a scan line are much greater than the observation dimensions at nadir (Fig. 1). The semivariograms of the reference data and simulated MODIS data from one ETM+ scene near nadir (0° < view zenith angle < 8°) and high view zenith angles (55° < view zenith angle < 65°) are presented in Fig. 8. Semivariograms plot a measure of variance as a function of distance and provide useful indications of the spatial variance of data. When comparing image data for different resolutions over the same area, semivariograms can be used as an indicator of the spatial information content of image data. The coarse resolution data has a lower sill value than the high-resolution data, which means it contains less spatial information. (Curran, 1988; Tian et al., 2002; Woodcock et al., 1997). The differences in semivariance related to view angle indicate a significant loss in spatial information content as view angle increases. The semivariance for the near nadir sensing scenario is within 10% of the reference data. However, at high view angles, the spatial information content of the image (using

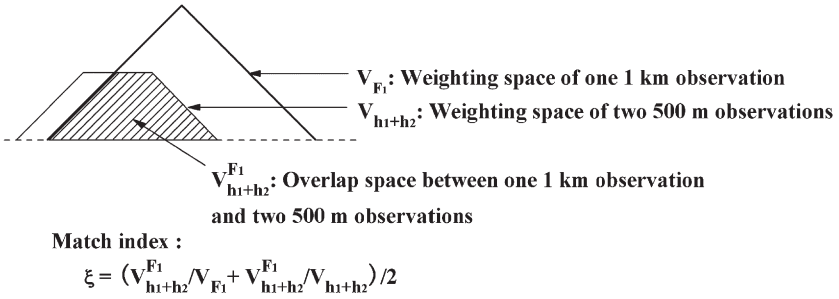

Fig. 5. The definition of the match index (ξ) is shown in a simple case — a single 1 km observation and two 500 m observations. In other cases, each weighting space can be the weighted aggregation result of multiple weighting spaces. Therefore, the general format of match index is $\xi = (V_{\sum\sum \alpha_j h_j}^{\sum \beta_i F_i} / V_{\sum \beta_i F_i} + V_{\sum\sum \alpha_j h_j}^{\sum \beta_i F_i} / V_{\sum \alpha_j h_j})/2$. The quantity α_i (β_j) is the weighting coefficient for the observation F_i (h_j) applied in the aggregation process.

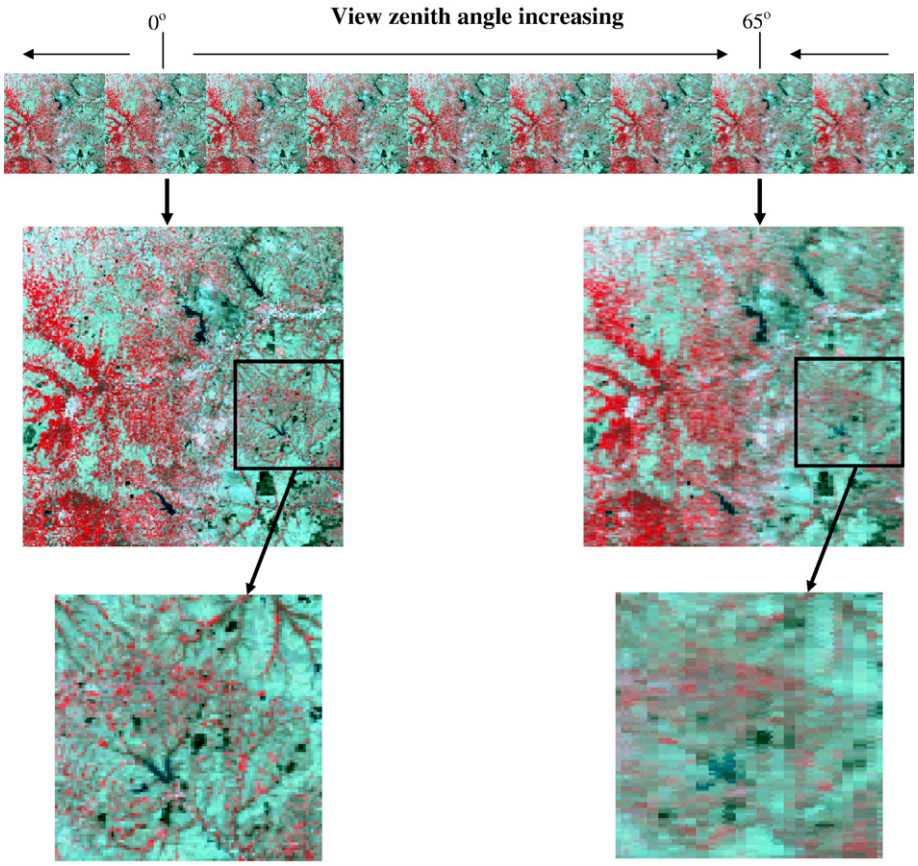

Fig. 6. Simulated MODIS data using the ETM+ data of the Konza Prairie LTER in April 04, 2000. The simulated MODIS data are at 500 m resolution. The images are a false color composite (RGB — near-infrared, red, and green bands, respectively). It can be seen that the image becomes blurred when the view zenith angle increases. This is because the observation dimensions are significantly greater than the cell dimensions, and one observation value is allocated to a number of adjacent grid cells. The top image was generated through duplicating the ETM+ image (147 by 147 km) 9 times and mosaicing them side-by-side.

semivariance as a measure of information content) is only about half of the reference data. As expected, as the observation dimensions increase, spatial variance will decrease, but the drop to 50% at the end of scan is dramatic.

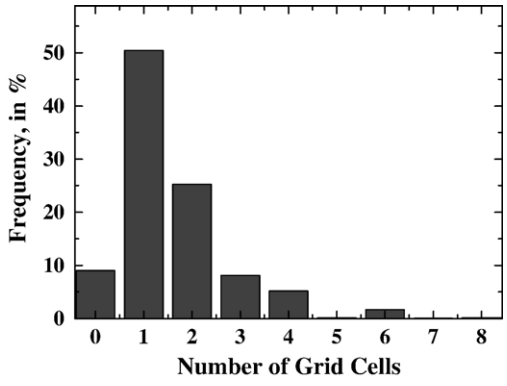

Fig. 7. The frequency distribution of the number of grid cells in the first layer to which single observations are assigned. Approximate 41% of the observations are allocated to multiple adjacent cells. An observation can be allocated to as many as 8 adjacent cells. Approximately 9% observations are not used in the output image because of the overlap between consecutive scan lines. A grid cell can be observed multiple times, but only one observation can be allocated to this cell. Therefore, some observations are not allocated to any cell.

For MODIS data, an observation in a grid cell is not necessarily sensed from the exact location the cell represents due to gridding artifacts. The surface area contributing to a MODIS observation is always larger than the cell size, even at nadir, due to the triangular PSF (refer to Section 3.2). In the best possible

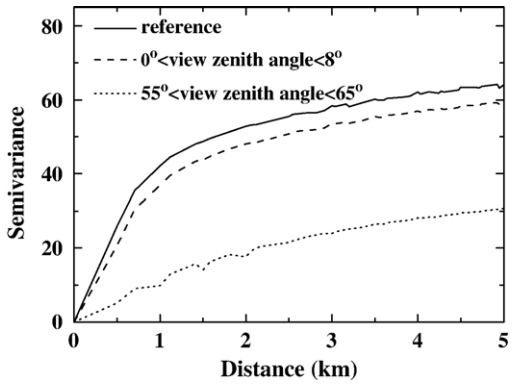

Fig. 8. Semivariograms of the reference data and the simulated MODIS data for the same location for observations near nadir and at the end of scan lines. The simulation is for Band 4 of the ETM+ data of the Konza Prairie LTER in April 04, 2000. At nadir, the spatial variance (or information content) is about 10% less than the reference data. At the end of scan, the spatial variability is only half of the reference image.

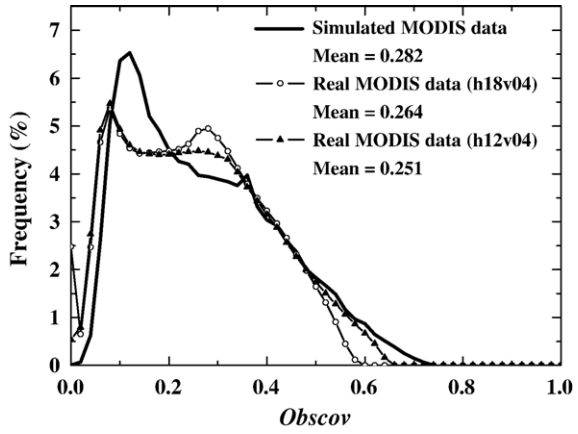

Fig. 9. The frequency distribution of obscov of 50 days of simulated MODIS data and of the Collection 4 MODPTHKM product in tile h18v04 and h12v04 from January 1st to February 19th, 2004. The similarity between the observed and simulated obscov distributions helps verify that the simulation is a good approximation of the real MODIS processing stream.

situation, or when the grid cell coincides exactly with its nominal observation (Fig. 2b), the area covered by a grid cell contributes 75% of signal to the observation assigned to it. The degree of correspondence between a grid cell and the observations in it is measured with obscov (Section 3.3). The frequency distribution of obscov for 50 days of simulated MODIS data is shown in Fig. 9 along with obscov for Collection 4 MODIS 500 m daily products for tile h18v04 and h12v04 from January 1st to February 19th, 2004. The frequency distributions of obscov for MODIS data and the simulated data are similar verifying that the simulation is a good approximation of the MODIS processing stream. It should be noted that the frequency

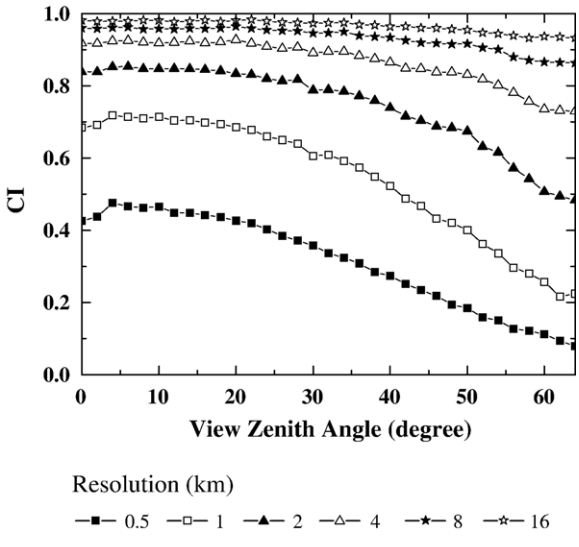

Fig. 10. The impact of view zenith angle and spatial resolution on obscov. Obscov increases as resolution decreases, and decreases with increasing VZA. The simple aggregation method is used to rescale the fine resolution data to coarse resolutions. The result shown here is the average of 50 days of simulations. Note that to have at least 80% overlap between the location of grid cells and their observations MODIS data needs to be aggregated by a factor of 8 (from 500 m to 4 km in this example) and high view zenith angles avoided.

distributions of obscov from real and simulated MODIS data are not exactly the same because we use a simplified model that excludes the following two factors: 1) the misalignment between the orientations of observations and grid cells, which limits the maximum possible obscov at nadir; and (2) there are gaps between two consecutive scan lines in real MODIS data, which lead to pixels with obscov values of 0.

The low correspondence between grid cells and the observations in them (mean obscov less than 30%, Fig. 9) has particularly significant implications for validation of MODIS algorithms with reference data. Comparison of MODIS data

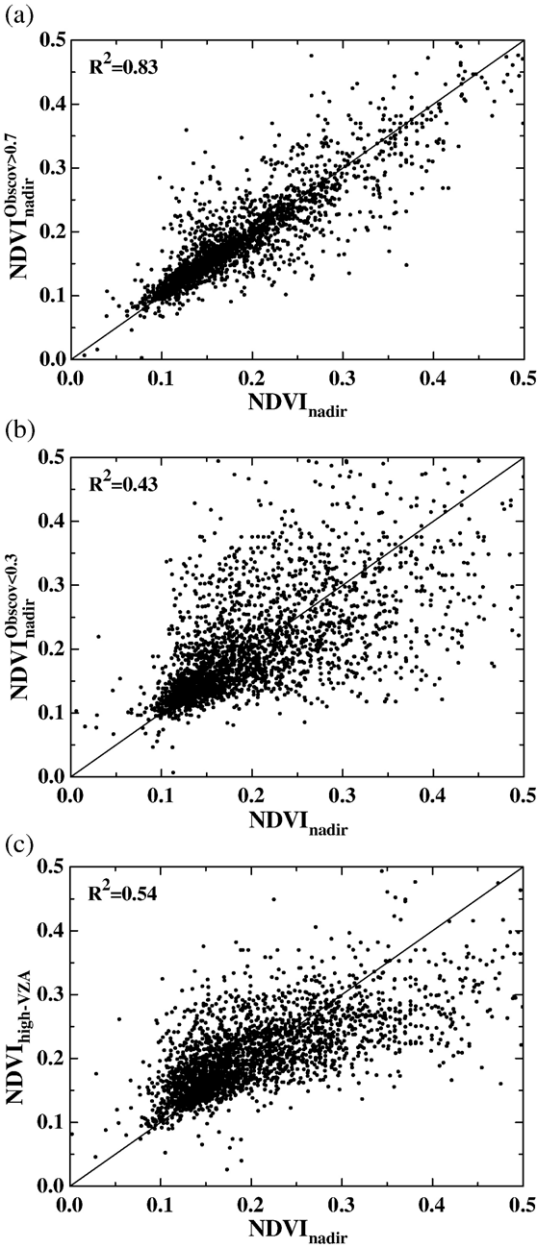

Fig. 11. NDVI of reference data versus NDVI of simulated data: (a) near nadir when obscov values are greater than 0.7; (b) near nadir when obscov values are less than 0.3; and (c) for high VZA regardless obscov. The cell by cell correspondence between values can be expected to be poor when obscov values are low. Reference data and simulated MODIS data are generated using the ETM+ data of the Konza Prairie LTER in April 04, 2000.

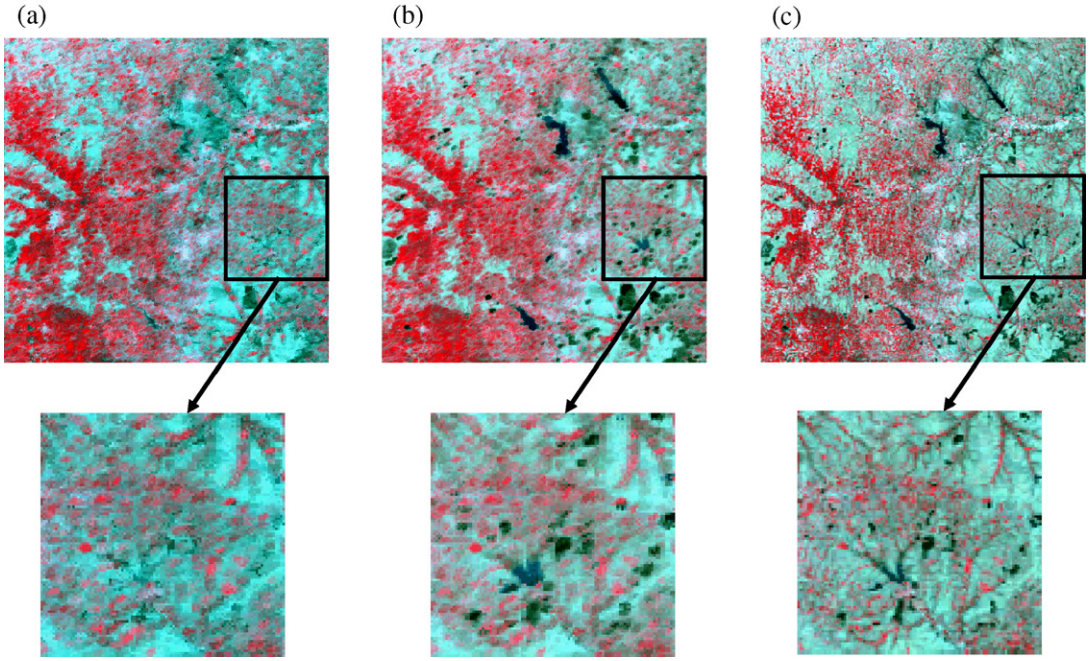

Fig. 12. The 8-day composite images from the compositing methods of (a) maximum NDVI, (b) minimum blue, and (c) minimum VZA. The simulated MODIS data are derived from the ETM+ data covering 147 by 147 km around the Konza Prairie LTER in April 04, 2000. Notice that the different compositing methods produce quite different results. Most noticeably, the maximum NDVI approach expands the sizes of the patches of vegetation (the red areas, or dark grey areas in b&W image) in (a), and the minimum blue approach expands the size of water bodies (black areas) and vegetation patches. The minimum VZA represents the "ground truth" in this case, as the lack of clouds results in nadir observations always being available.

products with reference data for a cell can be misleading because they generally will not be from the same location. For "product validation" (see the definition in Section 1) this issue is not terribly relevant, as the mismatch between grid cells, reference data and observations is one of many factors contributing to product inaccuracy. But for "algorithm validation", it is important that reference data and observations match. From the results shown in Fig. 9, it is clear that in general they do not match. So other alternatives are required to perform cell-by-cell comparisons. One possibility is to use the geolocation data provided with MODIS products to take into account the effects of pixel shift. This approach has the advantage of improving the locational accuracy of individual MODIS observations. But it is important to remember that this approach does not solve this problem entirely as the effects of geolocation error will still exist. Another option is to aggregate the data, which tends to improve obscov (see Fig. 10). It is worth noting that an average obscov of 80% can be achieved by aggregation to 8 times the native resolution (or 2 km for the 250 m bands).

Another way to explore the effect of obscov on MODIS data quality is cell by cell comparison of NDVI values between the reference data and the simulated MODIS data (Fig. 11). The cells near nadir with obscov > 0.7 or obscov < 0.3 are compared with reference data separately. As expected, there is better correspondence between reference and simulated MODIS data ($R^2 = 0.83$) when obscov values are high (Fig. 11a), and poor correlation ($R^2 = 0.43$) when obscov values are small (Fig. 11b).

In MODIS data, the obscov values of adjacent cells can be quite different. This spatial variability in obscov is due to misalignment and mismatch between observations and grid cells. The spatial distribution pattern of obscov differs from one place to another, and depends on the alignment between the orientation of observations and grid cells. The comparison between reference data and simulated MODIS data at the end of a scan line is shown in Fig. 11c. The correlation is poor ($R^2 = 0.54$). The NDVI dynamic range in the reference data is larger than in the simulated MODIS data. This "blurring" effect

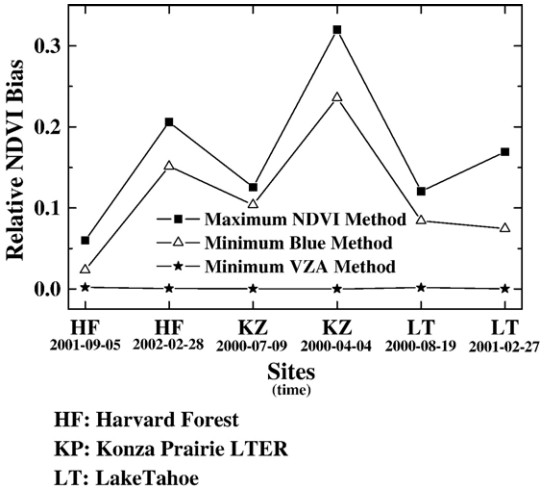

Fig. 13. The relative NDVI bias ($\Delta NDVI/NDVI_{True}$) in 8-day composite data using the maximum NDVI, minimum blue, and minimum VZA methods. Results are shown in six sets of data — Harvard Forest on 09/05/2001 and 02/28/2002, Konza Prairie LTER on 07/09/2000 and 04/04/2000, and Lake Tahoe on 08/19/2000 and 02/27/2001. Maximum NDVI and minimum blue compositing methods lead to positive bias in NDVI, while minimum VZA shows negligible bias.

in MODIS is due to the growth of the observation dimensions near the end of scan lines, as illustrated in Fig. 6.

4.2. The effect of gridding artifacts on compositing

To evaluate the effect of gridding artifacts on different compositing methods, three methods are investigated in this study through simulation: (1) maximum NDVI, (2) minimum blue and (3) minimum VZA. The maximum NDVI compositing method was selected because it is the legacy method used for processing AVHRR data (e.g. Maselli et al., 2003; Myneni et al., 1998). The minimum blue method was used to generate the Collection 3 8-day composite MODIS surface reflectance product. It was replaced by the minimum VZA method in Collection 4 reprocessing. It should be noted that all ETM+ data used in this study are cloud free. Therefore, the effects of clouds and bad observations are not considered here. Fig. 12 shows the images generated by the three compositing methods. Comparison with the daily nadir image (Fig. 6) reveals the following trends: 1) the minimum blue and maximum NDVI methods lead to "blur" in the 8-day composite data because they preferentially select off-nadir observations (Roy, 2000); 2) the vegetated areas (the red areas in the image) increased in size in the minimum blue and maximum NDVI results; 3) the small towns (bright areas) in the image disappear or shrink in the images using minimum blue and maximum NDVI for compositing; 4) the water

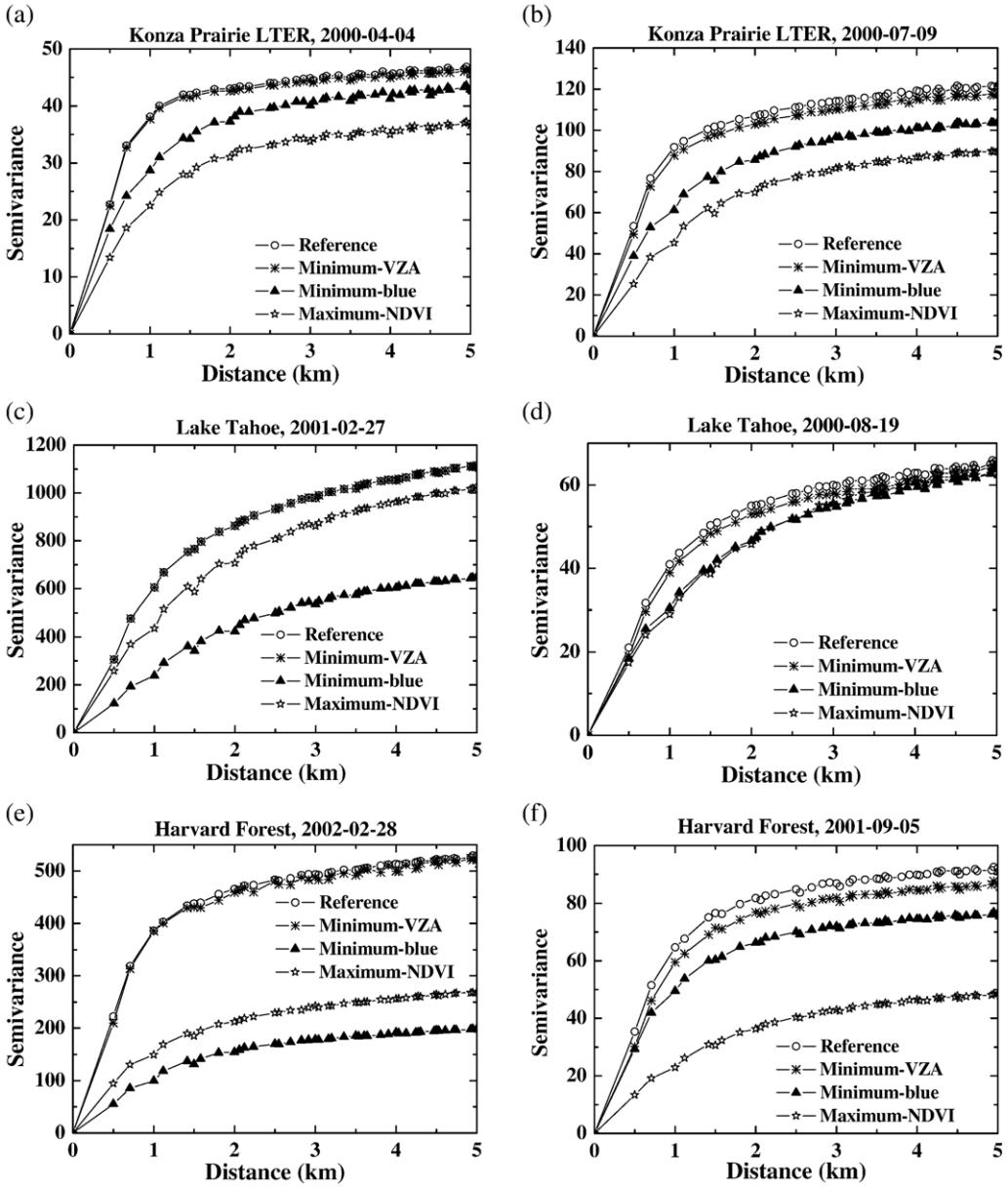

Fig. 14. Semivariograms of the near-infrared band of reference data and 8-day composites which are composited by maximum NDVI, minimum blue, and minimum VZA methods. Results are shown in six sets of data — Harvard Forest on 09/05/2001 and 02/28/2002, Konza on 07/09/2000 and 04/04/2000, and Lake Tahoe on 08/19/2000 and 02/27/2001. The current method used by MODIS (minimum VZA) seems to be very close to the simulated reference data. The maximum NDVI and minimum blue composite methods tend to select high view zenith angle data. As mentioned before, since these high view zenith angle data have coarse spatial support (observation dimensions), their spatial variability decrease with respect to the reference data.

areas (dark areas) shrink in maximum NDVI result, while the minimum blue result is more complicated. The water area shrinks if the water is surrounded by dense vegetation, which has lower blue reflectance. Otherwise, the water area expands using the minimum blue criterion; and 5) the minimum VZA compositing is the best, and keeps most of the ground information.

Fig. 13 shows the NDVI bias, calculated as the difference between the mean composited NDVI minus the mean reference NDVI divided by the mean reference NDVI, for the three compositing methods in six sets of simulated MODIS data. The true NDVI value is calculated from the reference image. The results of the maximum NDVI and minimum blue methods overestimate NDVI, while the result of minimum VZA method is almost exactly the same as the true NDVI value. The magnitude of the bias depends on the ground conditions. The maximum NDVI and minimum blue composites have less spatial variability (or signal) than the minimum VZA result primarily due to the blurring effect of tending to select high view zenith angle data in the composites (see Figs. 8 and 14). For the simulated data with no clouds, the minimum VZA results are very close to the reference data but not exactly the same as the reference data because the view zenith angle for the reference data is always zero, which is not the case for the simulated data. It is interesting to note that the magnitude of the NDVI bias and the degree of blurring (or decrease in spatial variability) related to the minimum blue and maximum NDVI compositing methods vary greatly as a function of the spatial fragmentation (Figs. 13 and 14). The spatial fragmentation varies significantly in both space and time. It should be noticed that the minimum VZA results may not closely match the reference data for real MODIS data and will vary from one multidate composite to another because the availability of cloud-free observations from near nadir will vary.

Fig. 15 presents the cell by cell comparisons of NDVI between reference data and simulated 8-day composite MODIS data for the different compositing methods. The results of maximum NDVI and minimum blue are poorly correlated with the reference data ($R^2=0.42$ and 0.35 respectively) due to the "blurring" effect of the compositing process. The result of minimum VZA correlates best with the reference data ($R^2=0.62$). The overestimates of the maximum NDVI and minimum blue results can be seen from these scatter plots. Similar to the daily data (Section 4.1), a better correlation between 8-day composite data and reference data can be expected at coarser resolutions. However, the overestimates of the maximum NDVI and minimum blue methods cannot be eliminated by aggregation.

The advantage of using spectral criteria for compositing derives from the ability to avoid clouds and bad observations. However, bias in the data and spectral indices like NDVI is an important shortcoming for such methods as it dramatically reduces the utility of the data for temporal comparisons. If accurate cloud masks are available, a spectrally independent compositing criterion, such as view zenith angle, will minimize bias in composited data.

In essence, to directly compare composited data over time to monitor global change requires consistency in the following: (1) sensing scenarios (view angle distribution and sensing frequency), (2) compositing methods, and (3) cloud frequency. Changes in any of these factors will complicate the ability to track changes in metrics like NDVI through time as sensing and processing artifacts will be convolved with possible change in surface conditions.

4.3. Impact on band-to-band registration

As mentioned in Section 3.6, the band-to-band registration across the native resolutions of MODIS data is strongly influenced by whether or not the finer resolution data are

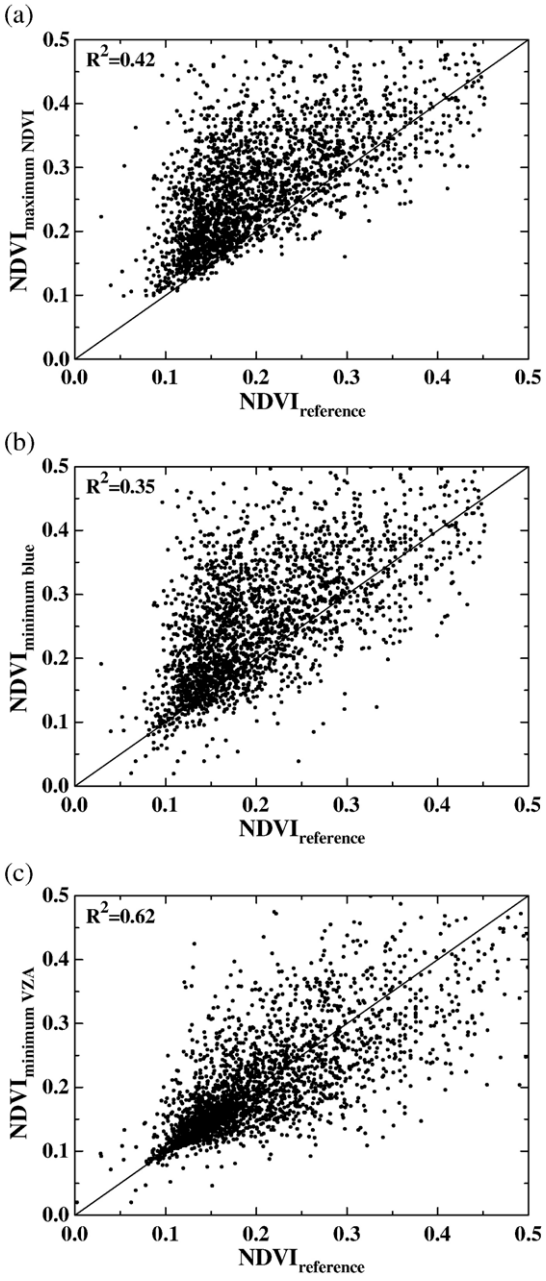

Fig. 15. NDVI of the reference data versus NDVI of 8-day composites generated with (a) maximum NDVI, (b) minimum blue, (c) minimum VZA. Note the weak correlation and overestimation bias of the maximum NDVI and minimum blue methods.

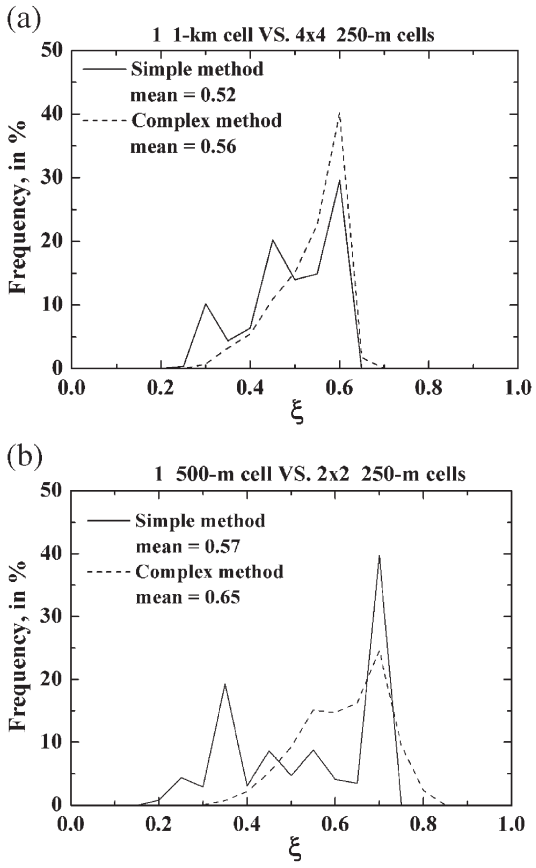

Fig. 16. The frequency of the match index (ξ) in half a swath area of (a) native 1 km data and 1 km data aggregated from 250-m, and (b) native 500 m data and 500 m data aggregated from 250 m. Both the simple and complex aggregation methods are presented. The aggregations using the complex method have a higher ξ than those using the simple method. However, it should be noted that the band-to-band registration across resolutions for MODIS data is poor compared to conventional multispectral observations.

gridded prior to aggregation. If the aggregation occurs prior to gridding and the weighting indicated in Section 3.6 is used, then there is a perfect band-to-band registration across resolutions. However, if the finer resolution data are gridded prior to aggregation, there will be some degree of mismatch between the different resolutions of imagery. To explore the magnitude of this effect, two aggregation methods, the simple and complex methods (explained in Section 3.4), are applied on the multi-layer data produced by the simple gridding method. The frequencies of the *matching index* (ξ) (Section 3.6) in half a swath of four situations are shown in Fig. 16: native 500 m data from the simple and complex methods vs. aggregated 500 m from 250 m data by both the simple and complex method, native 1 km data from simple (complex) method vs. aggregated 1 km from 250 m data by simple (complex) method. The mean ξ of four situations ranges from 0.52 to 0.65. Values of ξ from the complex method are slightly higher than those from the simple method. Such low values for the *matching index* indicate that: (1) the native coarse resolution MODIS products are not directly comparable to the aggregated MODIS products from gridded finer resolution MODIS data; (2) fine resolution MODIS products should be used with care to analyze the subpixel dynamics of coarse resolution MODIS products as the fine resolution observations do not come from the same locations as the coarse resolution observations.

The semivariograms of the 1 km aggregated data of the near-infrared band using nadir (high view zenith angle) data are shown in Fig. 17. At nadir, the 1 km data aggregated from 250 m and 500 m contain similar amounts of spatial information. However, at high view zenith angles the 1 km data from native 500 m data contain approximate 30% less spatial information than the 1 km data from native 250 m data.

4.4. Discussion

The gridding artifacts together with the effects of viewing geometry undermine the local spatial properties of MODIS data and have implications in many domains. For validation of MODIS algorithms, direct comparison of reference data on a pixel-by-pixel basis with MODIS products will introduce error unrelated to the algorithm (Figs. 9 10 and 11). Two alternatives are recommended to reduce the effect of gridding artifacts. The first is

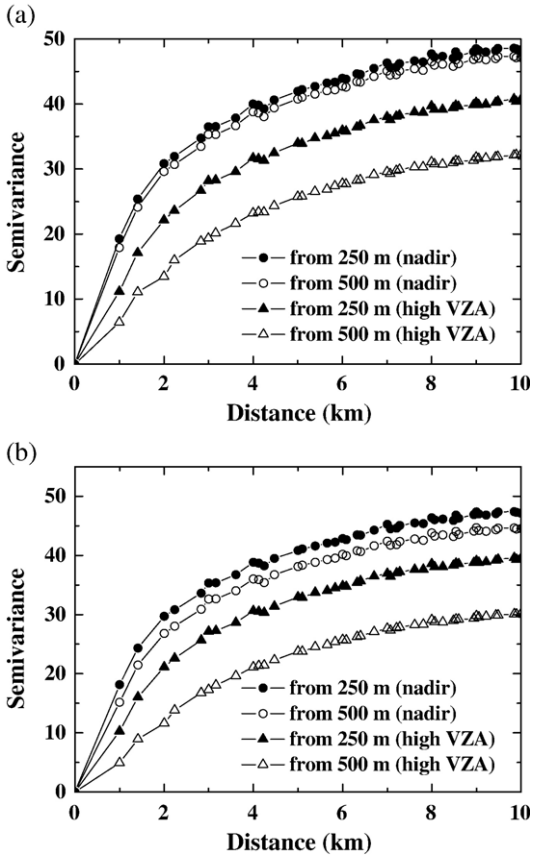

Fig. 17. The semivariograms of 1 km resolution data, which are aggregated from 250 m and 500 m data, at nadir and high VZA. Panel a shows results from the simple method, while panel b is from the complex method. At nadir, the 1 km data aggregated from both 250 m and 500 m data contain the same amount of the spatial information. However, for high VZAs, the 1 km data resulting from aggregation of 250 m data contain approximate 30% more spatial information than the 1 km data from native 500 m data. The results of the complex method contain slightly less spatial information than the results of simple method due to the blurring effect of weighted averaging.

to utilize the detailed geolocation information about MODIS observations stored in MODIS level 2 products, including the obscov value, the dimensions of the observation and the offset between the grid cell and the observation. The ground area covered by an observation can be more accurately located using this information than the location of the grid cell. In such a way, the comparison between field data and MODIS products is more reliable. However, it is important to note that using this approach will not allow for perfect alignment of ground reference data and MODIS observations as geolocation error will still be present. The second approach, when detailed data are not available, is to compare them at a coarser resolution (e.g. patch level) rather than the native resolution. For this approach, the validation site should be large to minimize the effect of gridding artifacts and to minimize the noise associated with individual observations.

Gridding artifacts also bring to light some of the difficulties associated with multidate compositing, as bias can be introduced through the use of spectral criteria for selection of the best observations (Figs. 13 and 15). These problems influence not only validation but also other applications of MODIS products. The spatial and/or spectral biases reduce the utility of MODIS products. The bias changes as a function of the spatial fragmentation (Figs. 13 and 14). The relationship between compositing bias and fragmentation could be characterized through analysis of enough ETM+ scenes to capture the full range of spatial fragmentation conditions. This is a direction of future studies.

The concept of a multispectral vector, in which observations from different wavelengths are collected for the same location, is central to remote sensing. However, this concept is undermined in some MODIS products due to the poor band-to-band registration (mean matching index of about 0.6) between the bands whose native resolutions are different if the data were gridded prior to aggregation (Fig. 16). This problem also limits the ability to use the fine resolution MODIS data (e.g. 250 m) to study the subpixel properties of the coarse resolution MODIS data (e.g. 1 km).

One of the key limitations with MODIS data concerns the increasing observation dimensions with increasing view zenith angle (Fig. 1). This problem can be minimized if a pushroom sensor is used rather than a scanner. The Charge Coupled Device (CCD) of the pushroom sensor should be designed such that the angular field of view decreases toward to the edge of the CCD and the pixel size on the ground remains constant. In such a way, a constant observation area on the ground can be achieved regardless of the view geometry. The use of a push-broom sensor would also remove the complications and problems associated with a triangular PSF, as illustrated in Fig. 2a. However, it should be noted that this kind of sensor will still suffer from the effects of gridding artifacts unless repeat observations can be guaranteed over the exact same area, which is improbable using current technology.

Most of the issues addressed in this paper result from the inherit properties of the MODIS sensor, and cannot be improved by changes in the processing stream. The teams responsible for designing, implementing, and modifying the processing stream have done an excellent job and deserve recognition. Of particular note in this regard is their change to minimum VZA compositing and modification to obscov. However, the poor band-to-band registration of MODIS data can be minimized with improved processing procedures. If the ungridded observations in different resolutions are gridded independently, the band-to-band registration across resolutions suffers due to gridding artifacts (e.g. MOAGAGG). A better method is to aggregate the ungridded observations from fine resolution to coarse resolution before gridding them (e.g. MOD09GHK). This approach results in perfect band-to-band registration between ungridded observations whose native resolutions are different (Fig. 4). The fine resolution ungridded observations can be aggregated to the coarse resolution without decreasing the precision of band-to-band registration (Section 3.6, Fig. 4). Then the aggregated and native coarse resolution data are gridded simultaneously. In such a way, the band-to-band registration problem can be minimized. However, the data with different resolutions are still not comparable because the band-to-band registration is degraded by the gridding process. It is impossible to find the original fine resolutions observations that correspond to a single coarse resolution observation.

5. Conclusions

The gridding process for MODIS data unavoidably results in a significant pixel shift effect that when combined with geolocation error results in a weak relationship between the location of grid cells and their observations. The mean obscov for a single date of MODIS data is less than 0.3. This relationship is particularly problematic at high view zenith angles where obscov can be as low as 0.05. These gridding artifacts have the following effects: First, direct comparison of reference data such as field measurements with MODIS data at the pixel scale is problematic because there will be a spatial mismatch between the locations of the observations and the reference data. There are two ways to maximize the correspondence of the ground area covered by both the field data and the MODIS data: 1) including obscov, the observation dimensions, and the offsets between the grid cell and the observation in validation analysis to retrieve a more accurate representation of observation coverage; or 2) aggregate MODIS data to improve the correspondence between the location of grid cells and the observations assigned to the cell. Second, the use of multidate compositing criteria based on spectral properties results in significant biases due to gridding artifacts. Third, under the practice of independent gridding of the various spatial resolutions of data, the band-to-band registration of bands with different native resolutions is poor (a mean matching index of about 0.6). This problem plagues some MODIS products and can be mitigated by a change in the processing procedure such that fine resolution bands are aggregated prior to gridding.

The results presented are based on simulations that capture the primary effects involved in gridding artifacts. However, the simulation process is not perfect and run only for 45° latitude. Because of the assumptions in the simulation (Section 3.5), the magnitude of the effects due to the gridding artifacts will be slightly underestimated. Exploring the effects of gridding artifacts as a function of latitude is a future research direction.

Acknowledgements

The authors thank Robert E. Wolfe and Eric F. Vermote at University of Maryland, Kamel Didan at University of Arizona, and Zhengming Wan at University of California at Santa Barbara for providing detailed MODIS algorithm and processing descriptions. We are also grateful for valuable comments from Jeffrey L. Privette of NASA GSFC, and two rounds of thorough anonymous reviews.

Appendix A. Calculation of the temporal orbit pattern of Terra

The period of the Earth rotation is approximately 86,164.1 s (23 h, 56 min, 4.1 s). The period of EOS Terra is about 5920 s (1 h, 38 min, 48 s). Therefore, the longitude distance (in degrees) between adjacent orbits is

$$360\textcircled{\$} \times \frac{5920}{86164.1} = 24.77\textcircled{\$}$$

We assumed the satellite begins at h degrees longitude. When EOS Terra finishes n full periods, the longitude coordination (H) is:

$$H = h + n \times 24.77$$

This approach is used to estimate the temporal orbit pattern. The distance D (km) between two longitude coordinates (lon_1 *and* lon_2) for a given latitude is derived as:

$$D = (\mathrm{lon}_1 - \mathrm{lon}_2) \times p$$

where p is the distance of 1° longitude for the given latitude.

Appendix B. Calculation of the observation dimensions/ observation bounding coordinates according to the scan angle

This Appendix shows how to calculate the observation dimension/observation bounding coordinates according to the scan angle, assuming 1) the Earth is a perfect sphere with a radius 6378.1 km. 2) the Earth curvature is reasonably ignored within an observation (the dimension ranges from 0.5 km by 0.5 km at nadir to approximately 4 km by 2 km at the end of a scan line). The field of view (FOV) in along-track/along-scan direction is calculated as:

$$\mathrm{FOV}_{\mathrm{track}} = \mathrm{FOV}_{\mathrm{scan}} = 2 \times \arctan \frac{dimension_{\mathrm{observe-at-nadir}}/2}{\mathrm{height}_{\mathrm{satellite}}}$$

where $\mathrm{dimension}_{\mathrm{observe\text{-}at\text{-}nadir}}$ is the spatial resolution of simulated MODIS data (250 m, 500 m, or 1 km); $\mathrm{height}_{\mathrm{satellite}}$ is 705 km. The following figure shows an off-nadir observation (EFGH) which is collected by the sensor. The known information in this figure is:

A the satellite position,
B the center of the Earth is B,
C the center of the observation boundary EF,
O the point sensed by the sensor center,
CD is perpendicular to AB at point D,
$\angle BAO$ the scan angle,
EF is perpendicular to the plane ACB,
A, O, C, D are in the same plane.

The length of AB equals the sum of the radius of earth (6378.1 km) and the height of the satellite (705 km).

E, F, G, H, G, O, C are on the surface of the Earth, which means $BE=BF=BH=BG=BC=6378.1$ km

$\because$ EF is perpendicular to the plane ACB, and $CD \subset \mathrm{Plane}_{ACB}$
$\therefore$ $EF \perp CD$
$\because$ C is the mid-point of EF and O the point sensed by the center of the sensor,
$\therefore$

$$\angle CAO = \frac{1}{2}\mathrm{FOV}$$

$\therefore$

$$\angle BAC = \angle BAO - \angle CAO = \mathrm{scan\_angle} - \frac{1}{2}\mathrm{FOV}$$

$\therefore$

$$\angle ACB = \pi - \arcsin\frac{AB \times \sin\angle BAC}{BC}$$

($\angle ACB$ is always larger than $90\textcircled{\$}$)

$\therefore$ $\angle ABC = \pi - \angle ACB - \angle BAC$
$\because$ $CD \perp AB$
$\therefore$ $CD = BC \times \sin\angle ABC$
$\therefore$

$$AC = \frac{CD}{\sin\angle BAC}$$

$\because$ $AC \perp EF$
$\therefore$

$$CE = AC \times \tan\angle EAC = AC \times \tan\left(\frac{1}{2}\mathrm{FOV}\right),$$

$\therefore$

$$EF = 2 \times CE,\ AE = \sqrt{AC^2 + CE^2}$$

Similarly, we can derive AF, AG, AH, and HG. Then FG and EH can be calculated as:

$$FG = \sqrt{AF^2 + AG^2 - 2 \times AF \times AG \times \cos\angle FAG}(\angle FAG = \mathrm{FOV}),$$

$$EH = \sqrt{AE^2 + AH^2 - 2 \times AE \times AH \times \cos\angle EAH}(\angle EAH = \mathrm{FOV}).$$

With the observation dimensions, the bounding coordinates for all pixels in a scan line could be calculated from the following method. In the simulation, the scan angle increases from 0 to 55° with a step of FOV. Here the observation corresponding to the scan angle of n steps is named as the nth

observation. The observation bounding coordinates of the nth observation are derived from the observation dimensions of the nth observation and the observation bounding coordinates of the $(n-1)$th observation because $(n-1)$th and nth observations are adjacent and there is no gap between them. The bounding coordinates for the observation at nadir ($n=0$) is calculated from the at-nadir observation dimensions and the position of the satellite. Then, the observation bounding coordinates are calculated in succession from nadir to the end of a scan line.

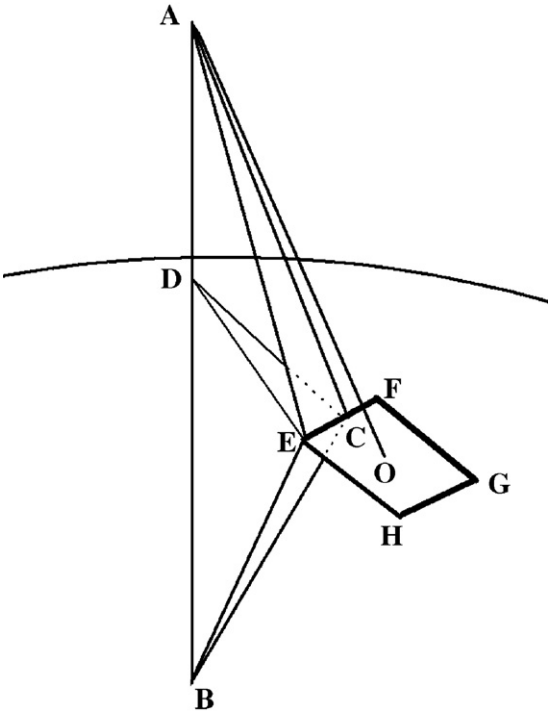

Fig. Calculation of the observation dimensions (*EFGH*) as a function of scan angle.

References

Barnes, W. L., Pagano, T. S., & Salomonson, V. V. (1998). Prelaunch characteristics of the Moderate Resolution Imaging Spectroradiometer (MODIS) on EOS-AM1. *IEEE Transactions on Geoscience and Remote Sensing*, *36*, 1088−1100.

Curran, P. J. (1988). The semivariogram in remote sensing: An introduction. *Remote Sensing of Environment*, *24*, 493−507.

Holben, B. N. (1986). Characteristics of maximum-value composite images for temporal AVHRR data. *International Journal of Remote Sensing*, *7*, 1435−1445.

Justice, C. O., Townshend, J. R. G., Vermote, E. F., Masuoka, E., Wolfe, R. E., Saleous, N., et al. (2002). An overview of MODIS land data processing and product status. *Remote Sensing of Environment*, *83*, 3−15.

Liang, S., Fang, H., Chen, M., shuey, C. J., Walthall, C., Daughtry, C., et al. (2002). Validating MODIS land surface reflectance and albedo products: Methods and preliminary results. *Remote Sensing of Environment*, *83*, 149−162.

Los, S. O., Justice, C. O., & Tucker, C. J. (1994). A global 1o by 1o NDVI data set for climate studies derived from GIMMS continental NDVI data. *International Journal of Remote Sensing*, *15*, 3493−3518.

Maselli, F., Romanelli, S., Bottai, L., & Zipoli, G. (2003). Use of NOAA-AVHRR NDVI images for the estimation of dynamic fire risk in Mediterranean areas. *Remote Sensing of Environment*, *86*, 187−197.

Moody, A., & Strahler, A. (1994). Characteristics of composited AVHRR data and problems in their classification. *International Journal of Remote Sensing*, *15*, 3473−3491.

Morisette, J. T., Privette, J. L., & Justice, C. O. (2002). A framework for the validation of MODIS Land products. *Remote Sensing of Environment*, *83*, 77−96.

Myneni, R. B., Tucker, C. J., Asrar, G., & Keeling, C. D. (1998). Interannual variations in satellite-sensed vegetation index data from 1981 to 1991. *Journal of Geophysical Research*, *103*, 6145−6160.

Nishihama, M., Wolfe, R. E., Solomon, D., Patt, F., Blanchette, J., Fleig, A., & Masuoka, E. (1997). *MODIS Level 1A Earth Location Algorithm Theoretical Basis Document.NASA Tech. Memo*. Greenbelt, MD: Goddard Space Flight Center SDST-092, Version 3.0.

Privette, J. L., Myneni, R. B., Knyazikhin, Y., Mukufute, M., Roberts, G., Tian, Y., et al. (2002). Early Spatial and Temporal Validation of MODIS LAI Product in Africa. *Remote Sensing of Environment*, *83*, 232−243.

Roy, D. P. (1997). Investigation of the maximum normalized difference vegetation index (NDVI) and the maximum surface temperature (T_s) AVHRR compositing procedures for the extraction of NDVI and T_s over forest. *International Journal of Remote Sensing*, *18*, 2383−2401.

Roy, D. P. (2000). The impact of misregistration upon composited wide field of view satellite data and implications for change detection. *IEEE Transactions on Geoscience and Remote Sensing*, *38*, 2017−2032.

Roy, D. P., Devereux, B., rainger, B., & White, S. (1997). Parametric geometric correction of airborne thematic mapper imagery. *International Journal of Remote Sensing*, *18*, 1865−1887.

Schowengerdt, R. A. (1997). *Remote sensing models and methods for image processing* (pp. 67–83) (2nd ed.). San Diego, CA: Academic Press.

Song, C., Woodcock, C. E., Seto, K. C., Lenney, M. P., & Macomber, S. A. (2001). Classification and change detection using Landsat TM data: When and how to correct atmospheric effects? *Remote Sensing of Environment*, *75*, 230−244.

Tan, B., Hu, J., Zhang, P., Huang, D., Shavanov, V. N., Weiss, M., et al. (2005). Validation of MODIS LAI product in croplands of Alpilles, France. *Journal of Geophysical Research*, *110*, D01107, doi:10.1029/2004JD004860.

Tian, Y., Woodcock, C. E., Wang, Y., Privette, J. L., Shabanov, N. V., Zhou, L., et al. (2002). Multiscale analysis and validation of the MODIS LAI product. I. Uncertainty assessment. *Remote Sensing of Environment*, *83*, 414−430.

Wan, Z., Zhang, Y., Zhang, Q., & Li, Z. (2002). Validation of the land-surface temperature products retrieved from Terra Moderate Resolution Imaging Spectroradiometer data. *Remote Sensing of Environment*, *83*, 163−180.

Wang, Y., Woodcock, C. E., Buermann, W., Stenberg, P., Voipio, P., Smolander, H., et al. (2004). Evaluation of the MODIS LAI algorithm at a coniferous forest site in Finland. *Remote Sensing of Environment*, *91*, 114−127.

Wolfe, R. E., Nishihama, M., Fleig, A. J., Kuyper, J. A., Roy, D. P., Storey, J. C., et al. (2002). Achieving sub-pixel geolocation accuracy in support of MODIS land science. *Remote Sensing of Environment*, *83*, 31−49.

Wolfe, R. E., Roy, D. P., & Vermote, E. (1998). MODIS land data storage, gridding, and compositing methodology: Level 2 grid. *IEEE Transactions on Geoscience and Remote Sensing*, *36*, 1324−1338.

Woodcock, C. E., Collins, J. B., & Jupp, D. L. B. (1997). Scaling remote sensing models. In P. R. Van Gardingen, G. M. Foody & P.J. Curran (Eds.), *Scaling-up from cell to landscape* (pp. 61−77). United Kingdom: Cambridge.

Yang, K., & Wolfe, R. E. (2001). MODIS leve 2 grid with the ISIN map projection. *IGARSS 2001: IEEE International Geosci. And Remote Sens. Symposium, Scanning the Present and Resolving the Further Proceedings*, *vols. 1–7* (pp. 3291–3293).